Distribution of mass, kinetic energy, and neutron yield in the spontaneous fission of ^{254}Fm†

J. E. Gindler, K. F. Flynn, L. E. Glendenin, and R. K. Sjoblom
Chemistry Division, Argonne National Laboratory, Argonne, Illinois 60439
(Received 23 May 1977)

The mass distribution for spontaneous fission of ^{254}Fm was determined for both pre- and post-neutron-emission fragments. The post-neutron-emission (final) mass distribution was deduced from radiochemical measurements of 24 mass yields. Starting with an assumed distribution of neutron yield versus fragment mass, the pre-neutron-emission (initial) mass distribution and neutron-yield distribution were derived from the kinetic-energy measurements of the fragments and the final-mass distribution by an iterative method. These distributions together with distributions of fragment kinetic energy, total kinetic energy of both fragments, and average kinetic energy and average total kinetic energy as functions of fragment mass are presented. The results are discussed in terms of a scission-point model of fission.

[NUCLEAR REACTIONS, FISSION ^{254}Fm(sf); measured radiochemical mass yields, fragment E; deduced neutron yields, fragment mass and energy distributions.]

I. INTRODUCTION

Fragment-mass distributions derived from kinetic-energy measurements for ^{254}Fm (Ref. 1), ^{256}Fm (Ref. 2), and ^{257}Fm (Refs. 3 and 4) spontaneous fission (sf) and ^{255}Fm (Ref. 5) and ^{257}Fm (Ref. 4) thermal-neutron-induced fission (n,f) exhibit a transition from double-peaked (asymmetric) fission to single-peaked (symmetric) fission as the mass of the fissioning fermium nucleus increases, particularly if the excitation energy is enhanced by the capture of a neutron. Although most of these mass distributions have not been corrected for the effect of neutron emission and are therefore *provisional* mass distributions, the transition from asymmetry to symmetry as the most probable mode of fission is clearly demonstrated. This transition is also verified by the shapes of post-neutron-emission (final) mass distributions determined by γ-ray spectrometry and/or radiochemical methods for ^{254}Fm (Ref. 6) and ^{256}Fm (sf) (Ref. 7) and ^{255}Fm (Ref. 8) and ^{257}Fm (n,f) (Ref. 9).

In the present paper the results of both radiochemical and kinetic-energy measurements of the fission fragments for ^{254}Fm(sf) are reported. The present radiochemical (RC) measurements examine the final-mass yields in the region of symmetric mass division (valley) more closely than do the measurements of Harbour *et al.*[6] who measured only one yield (that of ^{127}Sb) in the valley. Kinetic energy (KE) measurements of the fragments were reported some time ago by Brandt *et al.*[1] However, this group did not have the advantage of the improved detector calibration method described by Schmitt, Neiler, and Walter.[10] Therefore, these measurements were repeated using the mass-dependent energy calibration procedure.[10] The neutron yield as a function of fragment mass and the pre-neutron-emission (initial) mass distribution were derived with an iterative method in which the final-mass distribution is compared with successive approximations of the initial-mass distribution deduced from the KE measurements.

II. EXPERIMENT

A. Fermium sources

^{254}Fm was separated from einsteinium sources containing a few percent by mass of ^{254}Es.[11] Separation was made on a Dowex-50 cation exchange column using α-hydroxy-isobutyric acid as the eluting agent. For RC measurements the purified fermium fraction was deposited on platinum disks. Two fermium sources were thus prepared, one with an initial ^{254}Fm(sf) activity of 5.2×10^{7} fissions/min and the other with 1.8×10^{6} fissions/min. The isotopic composition of the sources was determined by observing both the α and spontaneous fission decay of small aliquots of the purified fermium fractions and by α and fission analyses of the fermium sources several weeks after their preparation. About 2% of the initial α activity of the sources was attributable to ^{255}Fm. However, the half-life for ^{255}Fm(sf) is much longer than that for ^{254}Fm(sf). Therefore, the contribution of ^{255}Fm to the fission activity was negligible. Likewise, the contribution to sf activity by ^{250}Cf, the daughter of ^{254}Fm, was insignificant except for one experiment.[12,13]

For the KE measurements the purified fermium was passed through an isotope separator and de-

posited onto thin (90 $\mu g/cm^2$) nickel. To avoid penetration of the fermium ions into the nickel backing, a low collection potential (300 V) was used. The shape of the fermium deposit was elliptical with major and minor axes of 6 and 3 mm. The initial ^{254}Fm(sf) activity of this source was 2.8×10^5 fissions/min.

B. Radiochemical procedures

The fermium sources were covered with 0.005-cm thick aluminum fission fragment catcher foils for periods of several hours. The catcher foils were then dissolved in the presence of carriers, specific fission products were radiochemically purified, and thick samples were mounted for β counting in a calibrated, low-background (0.4 count/min), end-window counter with an anti-coincidence shield.[14] The radioactive purity of each sample was checked by following its decay, generally for several half-lives. The observed counting rate for each fission product was corrected for chemical yield, counter efficiency, decay, genetic relationships, and degree of saturation to give the relative saturation activity A^∞ which is proportional to the fission yield. The resulting values of A^∞ were plotted as a mass-yield curve and normalized to 200% total yield to give absolute fission yields.

C. Kinetic-energy measurements

The experimental equipment, arrangement, and electronics used in the present experiment were similar to those described by Reisdorf *et al.*[15] Coincident fission fragments were detected with two 4-cm^2 gold-surface-barrier silicon detectors. The resultant pulse heights were recorded event by event onto magnetic tapes which were subsequently processed off line. Post-neutron-emission kinetic energies of complementary fragments were calculated from the recorded pulse heights using the mass-dependent energy calibration[10] based on a ^{252}Cf fission fragment energy spectrum. Post-neutron-emission energies were transformed into pre-neutron-emission energies by correcting for the average effects of neutron emission from the fragments. Since the number of neutrons emitted as a function of fragment mass $\bar{\nu}(M)$ was not known for ^{254}Fm(sf), this function was derived with an iterative method in which successive approximations of the initial-mass distribution deduced from the kinetic-energy measurements were compared with the final-mass distribution.[2] The initial-mass distribution which is also a result of this iterative method was calculated from the pre-neutron-emission energies through the conservation laws of mass and linear momentum.

III. RESULTS AND DISCUSSION

A. Final-mass distribution

The fission yields determined for the 24 mass chains are presented in Table I. The error for each value was estimated on the basis of the number of measurements, errors in the determination of A^∞, and any uncertainties in the decay scheme of the particular nuclide measured. The fission yields are plotted as circles in Fig. 1. The curve drawn through the circles represents the final-mass distribution normalized to 200% total yield. Triangles in the figure represent the data of Harbour *et al.*[6] The agreement between the two sets of data (circles and triangles) is good. Mean masses (first moments) for the light and heavy mass groups ($\bar{A}_L$ and $\bar{A}_H$) are 108.8 and 141.3, respectively. The average number of neutrons emitted per fission $\bar{\nu}_T$, derived from the equation

$$\bar{\nu}_T = A_F - (\bar{A}_L + \bar{A}_H) \quad (1)$$

TABLE I. Fission product yields for ^{254}Fm(sf).

Fission product	Fission yield (%)	Number of determinations
^{91}Sr	0.38 ±0.04	1
^{93}Y	0.48 ±0.05	1
^{95}Zr	0.54 ±0.08	1
^{97}Zr	1.35 ±0.13	2
^{103}Ru	3.13 ±0.31	1
^{106}Ru	5.75 ±0.58	1
^{109}Pd	5.67 ±0.57	1
^{111}Ag	5.50 ±0.30	3
^{112}Pd	5.06 ±0.51	1
^{115g}Cd	4.47 ±0.44 [a]	1
^{115m}Cd	0.58 ±0.06 [a]	1
^{115}total chain	5.05 ±0.45	
^{121g}Sn	0.666±0.067 [a]	2
^{121}total chain	0.770±0.080 [b]	
^{125g}Sn	0.066±0.007 [a]	1
^{125}total chain	0.138±0.024 [c]	
^{127}Sb	0.240±0.03	2
^{129}Sb	0.880±0.09	2
^{131}I	2.58 ±0.26	1
^{132}Te	3.02 ±0.30	1
^{133}I	3.29 ±0.33	1
^{140}Ba	5.49 ±0.55	3
^{141}Ce	6.29 ±0.50	1
^{143}Ce	5.64 ±0.30	3
^{144}Ce	5.09 ±0.50	1
^{153}Sm	1.42 ±0.14	1
^{157}Eu	0.62 ±0.06	1
^{159}Gd	0.44 ±0.04	1

[a] Isomer yield.

[b] Total chain yield estimated by assuming isomer ratio $(m+g)/g$ of 1.16±0.11 (Ref. 16).

[c] Total chain yield estimated by assuming isomer ratio of 2.1±0.3 determined for ^{252}Cf(sf) (Ref. 17).

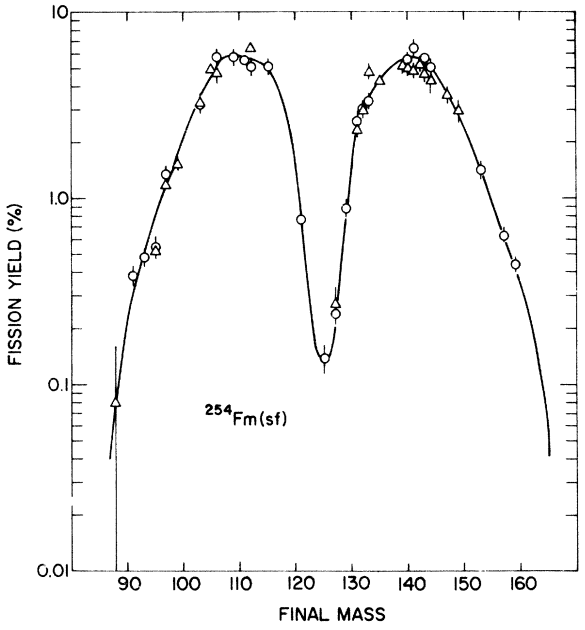

FIG. 1. Final-mass distribution for ^{254}Fm(sf) determined from radiochemical and γ-ray spectrometry measurements. Circles represent present data. Triangles represent data from Ref. 6. The solid curve represents a total yield of 200%.

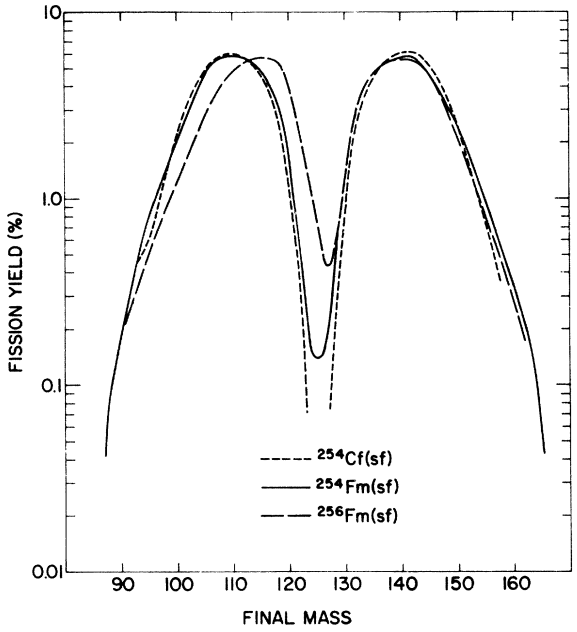

FIG. 2. Final-mass distributions for the spontaneous fission of ^{254}Cf, ^{254}Fm and ^{256}Fm.

in which A_F is the mass of the fissioning nucleus, is 3.9 with an estimated error of ±0.5. The accepted value of $\bar{\nu}_T$ by neutron counting[18] is 3.98 ± 0.14. The peak-to-valley ratio (P/V) of the final mass distribution is ~42.

^{254}Fm is isobaric with ^{254}Cf, isotopic with ^{256}Fm, and isotonic with ^{252}Cf and ^{253}Es, all of which undergo spontaneous fission. The final-mass distributions for these nuclides are compared in Figs. 2 and 3. In Fig. 2 the ^{254}Fm mass distribution (solid curve) is shown with those for ^{254}Cf (short-dashed curve)[19,20] and ^{256}Fm (long-dashed curve).[7] In Fig. 3 the mass distribution for the three isotones, ^{254}Fm (solid curve), ^{253}Es (long-dashed curve)[21] and ^{252}Cf (short-dashed curve),[17] are compared. The parameters $\bar{A}_L$, $\bar{A}_H$, $\bar{\nu}_T$, and P/V associated with the various mass distributions shown in Figs. 2 and 3 are listed in Table II. From Fig. 2 and Table II it is seen that the positions of the light- and heavy-mass groups, and consequently $\bar{A}_L$ and $\bar{A}_H$, for ^{254}Fm and ^{254}Cf are very similar. However, the values of P/V for the two fissioning systems are quite different. If one considers the isotones ^{252}Cf and ^{254}Fm, one observes that the addition of two protons causes the value of P/V to decrease by roughly a factor of 9. A similar but even larger result is observed if one considers the isotones ^{254}Cf and ^{256}Fm. If one now considers the isotope pairs ^{252}Cf-^{254}Cf and ^{254}Fm-^{256}Fm, one observes that the addition of two neutrons causes the value of P/V to decrease by a factor of about 3. Combining these crude results for the isobars ^{254}Fm and ^{254}Cf one would estimate that the addition of the two protons in ^{254}Fm would cause

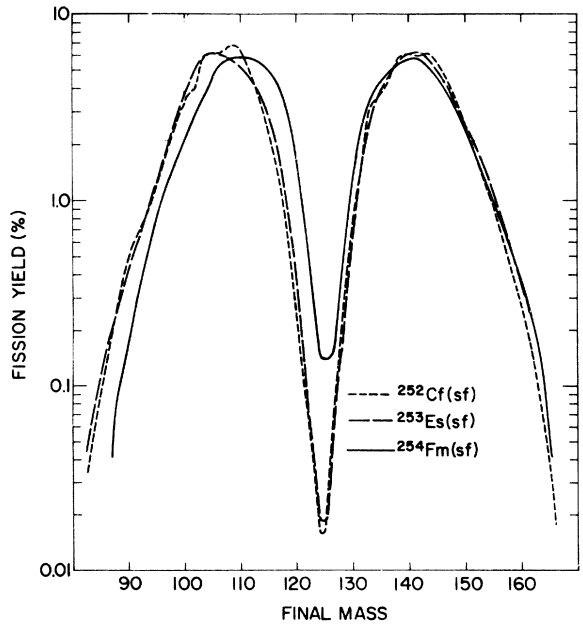

FIG. 3. Final-mass distributions for the spontaneous fission of the isotones ^{252}Cf, ^{253}Es, and ^{254}Fm.

TABLE II. Final-mass distribution parameters for several spontaneously fissioning systems.

Fissioning nuclide	$\bar{A}_L$	$\bar{A}_H$	$\bar{\nu}_T$ [Eq. (1)]	$\bar{\nu}_T$ (Measured)	P/V
^{252}Cf [a]	106.0	142.0	4.0	3.733 [b]	≥ 370
^{254}Cf [c]	108.6	141.5	3.9	3.89 [d]	≥ 145
^{253}Es [e]	105.9	142.4	4.7		326
^{254}Fm [f]	108.8	141.3	3.9	3.98 [d]	~42
^{256}Fm [g]	111.9	141.0	3.1	3.73 [h]	~12

[a] Data from Ref. 17.
[b] Preliminary recommended value added in proof from Ref. 18.
[c] Radiochemical data from Refs. 19 and 20.
[d] Value from Ref. 18.
[e] Data from Ref. 21.
[f] Values from present work.
[g] Data from Ref. 7.
[h] Value from Ref. 22.

a decrease in P/V by a factor of 9 or 10 compared with ^{254}Cf, but the fact that ^{254}Fm has two fewer neutrons would cause the value of P/V to increase by a factor of about 3, for an overall decrease in P/V of roughly 3. This estimate is in agreement with the experimental results.

In a recently developed scission-point model of fission, Wilkins, Steinberg, and Chasman[23] have shown that the stability of the heavy mass group can be accounted for by a strong fragment shell with ~88 neutrons and a β deformation of ~0.65 (Fig. 1 of Ref. 23). Furthermore, the value of P/V can be correlated with the potential energy difference between the mass split (142 + complement) and the symmetric mass split. For fissioning nuclides that lie approximately along the valley of β stability this potential energy difference exhibits a maximum at $A_F = 252$ (corresponding to a maximum P/V) and decreases as A_F increases to mass 262, in general agreement with the trends shown in Figs. 2 and 3 and outlined in Table II. Detailed calculations would be necessary to determine from the fission model[23] which specific fissioning isobar would exhibit the deepest valley yields.

B. Neutron emission function

The neutron-emission function $\bar{\nu}(M)$ for ^{254}Fm(sf) derived by the iterative method[2] is shown as the solid curve in Fig. 4. The function determined experimentally by Bowman *et al.*[24] for ^{252}Cf(sf) and the one deduced by the iterative method[2] for ^{256}Fm(sf) are shown for comparison as the dotted and dashed curves, respectively. All three curves exhibit the characteristic saw-toothed shape.

Maximum neutron emission in ^{254}Fm(sf) occurs at fragment masses 123–124 and minimum neutron emission at masses 129–130. The mass for which minimum neutron emission occurs is characteristic of all three neutron functions and is correlated with the low deformation, closed-shell structure of fragments with this mass. Maximum neutron emission occurs from masses which are complementary or nearly complementary to the mass from which minimum neutron emission occurs. Such a result is expected if the total deformation of both fission fragments is nearly constant since neutron emission is correlated with fragment deformation.[25] The near constancy of the total deformation of the fragments is indicated in the scission-point model of fission.[23] From the contour plot of the potential energy surface in Fig. 4 of Ref. 23 it is clear that fission fragments can deform more readily in the direction of constant total deformation than in an opposite direction in which both fragments become either more spherical or more deformed. For example, in the symmetric mass split of ^{236}U for one fragment to change from a β deformation of 0.62 to 1.0 and the other to change from 0.62 to 0.24 requires ~4 MeV of energy. For both fragments to change from β deformations of 0.62 to 1.0 requires ~7 MeV and for both to change from 0.62 to 0.24 requires ~10 MeV.

The average number of neutrons emitted per light (L) or heavy (H) fragment, calculated from the relationship

$$\bar{\nu}_{L,H} = \frac{\sum_{L,H} Y(L,H)\bar{\nu}(L,H)}{\sum_{L,H} Y(L,H)} , \qquad (2)$$

where Y represents the yield of the initial fragment, is 2.32 for the light fragment and 1.66 for the heavy fragment. Values derived from differences between first moments of the initial- and final-mass groups ($\bar{M}_{L,H} - \bar{A}_{L,H}$) are 2.2 for the light-mass and 1.7 for the heavy-mass groups.

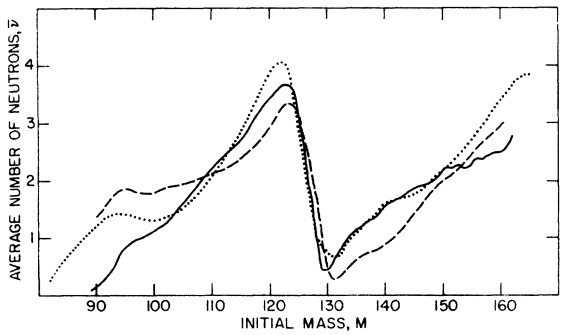

FIG. 4. Neutron yield as a function of initial mass for the spontaneous fission of ^{252}Cf (dotted curve, Ref. 24), ^{254}Fm (solid curve, present work), and ^{256}Fm (dashed curve, Ref. 2).

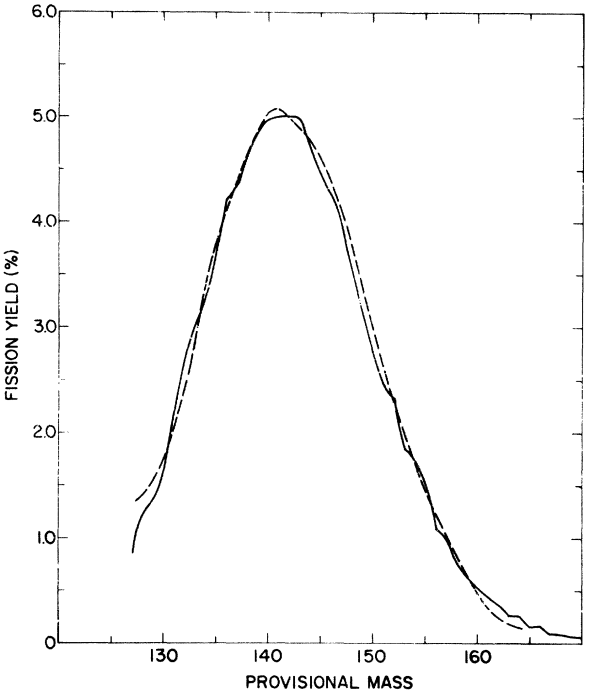

FIG. 5. Provisional mass distribution for ^{254}Fm(sf): solid curve (present work), dashed curve (Ref. 1).

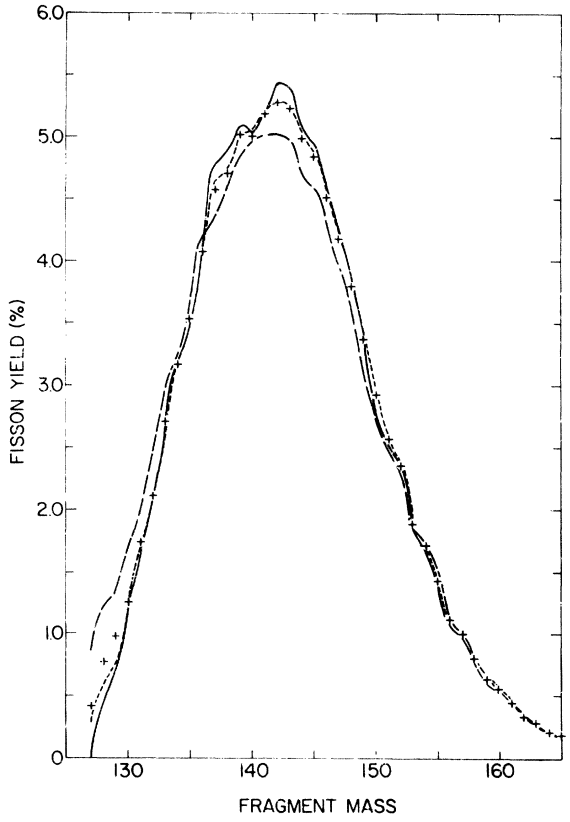

FIG. 6. Effect of various corrections in the calculation of the ^{254}Fm(sf) initial mass distribution. The long-dashed curve represents the provisional mass distribution. The short-dashed curve is the distribution obtained after correcting the kinetic-energy measurements for the emission of neutrons from the fragments. Crosses represent the yields obtained by correcting the short-dashed curve for the T_{KE} dependence of neutron emission with Eqs. (3)–(6). The solid curve represents the initial-mass distribution and is obtained by correcting for mass resolution the yields shown as crosses.

C. Mass distributions derived from kinetic-energy measurements

A *provisional* mass distribution (one in which no correction is made for neutron emission by the fragments) was deduced from the kinetic-energy measurements to compare the present results with those of Brandt *et al.*[1] Both distributions are plotted in Fig. 5 as the solid and dashed curves, respectively. The two distributions agree quite well; full widths at half maximum are 18 to 19 mass units for both; the peaks of the two curves are only one mass unit apart. However, the distribution obtained in the present work indicates some structure and has a somewhat lower value at symmetry than is indicated by the data of Ref. 1.

The effect of various corrections on the mass distribution derived from KE measurements is shown in Fig. 6. The provisional mass distribution is represented by the long-dashed curve. The mass distribution obtained by correcting the kinetic-energy measurements for the emission of neutrons from the fragments is given by the short-dashed curve. The crosses represent the mass yields obtained after a correction is made for the dependence of the number of neutrons emitted on the total kinetic energy released in the mass split, $T_{KE}(M)$. This dependence was calculated differently in four regions according to the difference between $T_{KE}(M)$ and the average total kinetic energy for the same mass split $\overline{T}_{KE}(M)$. If $\Delta T_{KE} = \overline{T}_{KE}(M) - T_{KE}(M)$, then for $\Delta T_{KE} \leq 0$ the relationship used for the number of neutrons emitted is

$$\nu(M, T_{KE}) = \overline{\nu}(M) + \frac{\overline{\nu}(M)}{\overline{\nu}(M) + \overline{\nu}(A_F - M)} \frac{\Delta T_{KE}}{\overline{E}_n^*}, \quad (3)$$

where $\overline{\nu}(M)$ is given by the solid curve in Fig. 4, A_F is the mass of the fissioning nucleus, and $\overline{E}_n^*$, taken to be 8.5 MeV, is the average sum of the binding energy and center-of-mass kinetic energy of the emitted neutron. Equation (3) with $\overline{E}_n^*$ taken to be 7.0 MeV is the $T_{KE}(M)$-dependence correction used in Refs. 2 and 15 for all values of ΔT_{KE}.

In the other three energy regions of ΔT_{KE}, the following relationships were used:

For $0 < \Delta T_{KE} < 20$ MeV,

$$\nu(M, T_{KE}) = \bar{\nu}(M) + \frac{M}{A_F}\,\frac{\Delta T_{KE}}{\bar{E}_n^*} \,. \tag{4}$$

For $20 \le \Delta T_{KE} \le 60$ MeV,

$$\nu(M, T_{KE}) = \bar{\nu}(M)\,\frac{60 - \Delta T_{KE}}{40} + \frac{M}{A_F}\,\frac{\Delta T_{KE}}{\bar{E}_n^*} + \frac{M}{A_F}\left[\bar{\nu}(M) + \bar{\nu}(A_F - M)\right]\left(1 - \frac{60 - \Delta T_{KE}}{40}\right). \tag{5}$$

For $\Delta T_{KE} > 60$ MeV,

$$\nu(M, T_{KE}) = \frac{M}{A_F}\left[\frac{\Delta T_{KE}}{\bar{E}_n^*} + \bar{\nu}(M) + \bar{\nu}(A_F - M)\right]\frac{\Delta T_{KE}}{60} \,. \tag{6}$$

Equations (4)–(6) have the effect of making neutron emission more proportional to the mass of the fragment as ΔT_{KE} increases. For $\Delta T_{KE} \le 60$ MeV some saw-toothed structure remains in the neutron yield function. Above 60 MeV, neutron emission becomes proportional to the mass of the fragment. In contrast, Eq. (3) alone magnifies the saw-toothed structure as ΔT_{KE} increases. The appropriateness of Eqs. (3)–(6) vs Eq. (3) alone was checked against values of $\nu(M, T_{KE})$ deduced from the measured neutron-emission data[24] for ^{252}Cf(sf). The use of Eqs. (3)–(6) gave considerably better fits than did the use of Eq. (3) alone. However, the effect of this correction on the mass distribution is very small.

The solid curve in Fig. 6 represents the distribution of initial-fragment-mass yields that is obtained by correcting the mass yields represented by crosses for mass resolution. The unfolding of the experimental mass yields to obtain resolution corrected yields was performed with an approximate iterative procedure[26] assuming the folding function to be a normalized Gaussian with a standard deviation $\sigma_D = 1.68$. The standard deviation was calculated with the equations given in Ref. 15 for the influence of the angular distribution of emitted neutrons on fragment recoil velocities, the energy resolution of the fragment detectors, and the energy loss of fragments in the target material. The derived initial-fragment-mass distribution thus reflects the extent to which the various assumptions made in the derivation are accurate.

The structure shown in the initial-mass distribution is peaked near masses 138–139 and 142–143. Structure found in other mass distributions (see, e.g., Ref. 2) has been attributed to a proton pairing effect and occurs at the average masses associated with even nuclear charges of $Z = 52$, 54, and 56 or their complements. These masses are related to nuclear charge by the relationships[2]

$$M_L = (Z_L - 0.5)(A_F/Z_F) \tag{7}$$

$$M_H = (Z_H + 0.5)(A_F/Z_F) \,. \tag{8}$$

For ^{254}Fm(sf) the masses associated with $Z = 52$, 54, and 56 are 133.4, 138.4, and 143.5, respectively. It therefore appears that the structural peaks in the ^{254}Fm(sf) initial-mass distribution are associated with $Z = 54$ and 56 or their complements. The first moments of the light ($\bar{M}_L$) and heavy ($\bar{M}_H$) mass groups are 111.0 and 143.0, respectively. The full width at half maximum for both groups is 17.3 mass units.

D. Kinetic-energy distributions

The kinetic-energy distributions for the light and heavy fragments and the total-kinetic-energy distribution for ^{254}Fm(sf) are shown in Figs. 7 and 8, respectively. The first moments and standard deviations also are given in the figures. The value of 195.1 MeV for $\bar{T}_{KE}$ is considerably larger than that determined by Brandt *et al.*,[1] 189 ± 2 MeV. These two values can be compared since a correction was applied in Ref. 1 for the average number of neutrons emitted. Values of $\bar{T}_{KE}$ obtained at this laboratory[2] for ^{248}Cm(sf), ^{250}Cf(sf), ^{252}Cf(sf), and ^{254}Cf(sf) are also consistently larger than the values in Ref. 1 (see Table III) and may be attributed to differences in calibration procedures. The present $\bar{T}_{KE}$ value for ^{254}Fm(sf) is ~3 MeV less than the value of 197.9 MeV for ^{256}Fm(sf).[2] This is opposite to the general trend that $\bar{T}_{KE}$ values increase with the Coulomb parameter $Z^2/A^{1/3}$ (see Table III) and has been discussed by Wilkins *et al.*[23] Their explanation for this phenomenon is

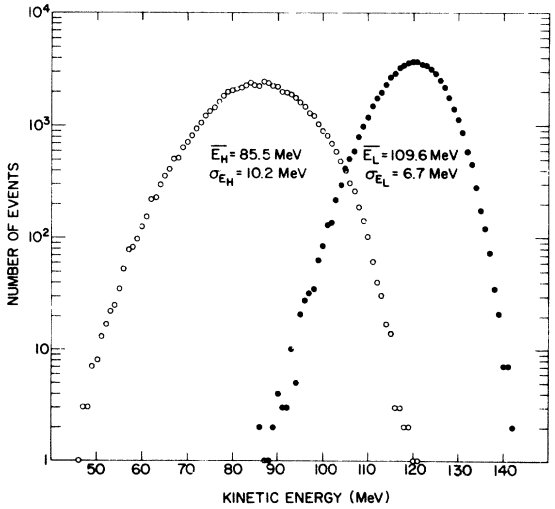

FIG. 7. The fragment-kinetic-energy distribution for ^{254}Fm(sf).

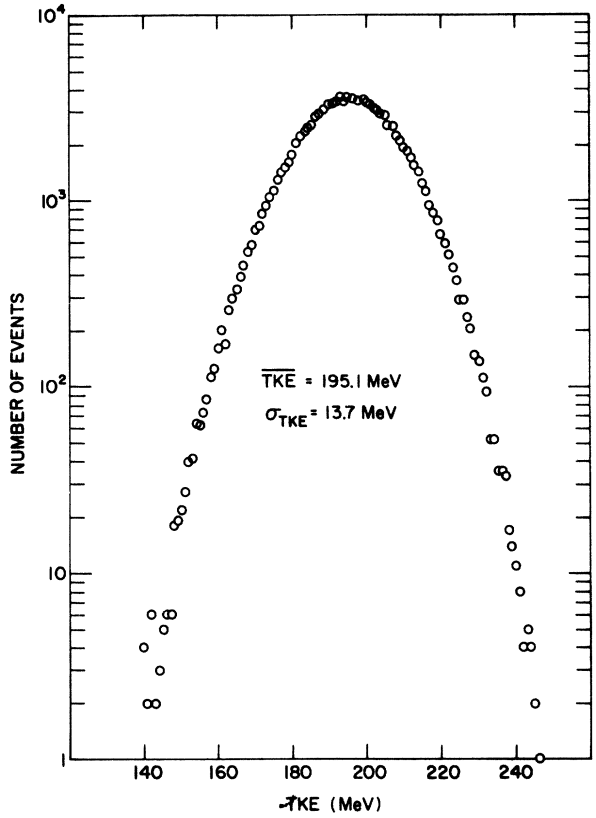

FIG. 8. The fragment-total-kinetic-energy distribution for ^{254}Fm(sf).

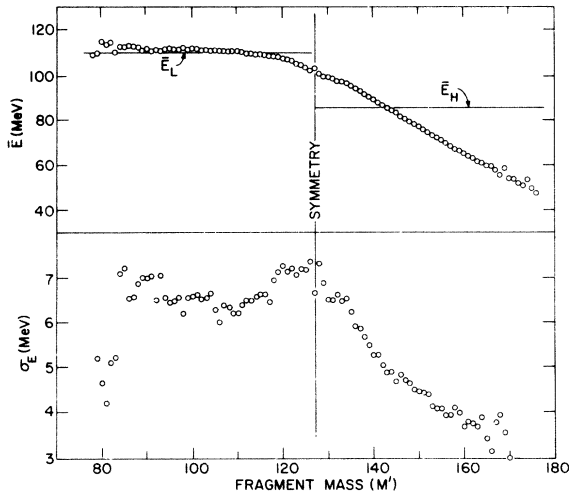

FIG. 9. The average kinetic energy $\bar{E}$ and the standard deviation of the kinetic-energy distribution σ_E as a function of mass for ^{254}Fm(sf). The distributions are uncorrected for experimental dispersion.

that the yield of the mass-symmetric component with fragment deformation near β values of 0.05 and 0.85 (points G and K in Fig. 1 of Ref. 23) increases rapidly with neutron number for isotopes of fermium. This configuration has a smaller total deformation than the typical asymmetric mass split and its contribution to $\bar{T}_{KE}$ will cause the value of $\bar{T}_{KE}$ to increase with increasing neutron number.

The average kinetic energy $\bar{E}(M')$ and the standard deviation of the kinetic-energy distribution

TABLE III. Average total kinetic energy released in spontaneous fission.

Fissioning nuclide	$Z^2/A^{1/3}$	T_{KE} (MeV) Ref. 1	Ref. 2
^{248}Cm	1466.9	179±2	182.2±0.9
^{246}Cm	1470.8		183.9±1
^{254}Cf	1516.5	185±2	186.9±1
^{252}Cf	1520.5	183±0.5	185.9±1
^{250}Cf	1524.5	185±3	187.0±1
^{253}Es	1549.6	188±3	
^{256}Fm	1574.9		197.9±1
^{254}Fm	1579.0	189±2	195.1±1 [a]

[a] Present work.

$\sigma_{E(M')}$ for a particular mass are plotted as a function of mass in Fig. 9. In both this figure and Fig. 10 the data are for masses that have not been corrected for mass resolution. The masses are therefore designated by M' to distinguish them from initial masses. In Fig. 9 one observes that $\bar{E}(M')$ for the light masses does not vary much compared to $\bar{E}(M')$ for the heavy masses. For masses >135, $\bar{E}(M')$ decreases ~1.2 MeV per mass unit. The variation in $\bar{T}_{KE}$ with M' shown in Fig. 10 is therefore attributable mainly to the variation of $\bar{E}(M')$ for the heavy fragment. Except for the value at $M'=127$, the $\bar{T}_{KE}(M')$ values (shown as open circles in Fig. 10) exhibit a slight decrease from $M'=133$ toward symmetry. This is in contrast to the $\bar{T}_{KE}(M')$ values for ^{256}Fm(sf) (Ref. 27) and ^{257}Fm(sf) (Ref. 3) for which $\bar{T}_{KE}(M')$ values increase from mass 133 toward symmetry. The reason for the latter effect is the same as that given for the increase in $\bar{T}_{KE}$ for ^{256}Fm(sf) relative to that for ^{254}Fm(sf). As the mass of the fissioning fermium nucleus increases, the complement of the spherical $M\sim132$ fragment approaches symmetry and its shape is determined[23] largely by a neutron shell with a β deformation of ~0.85. This configuration represents a smaller total deformation than is found for symmetric mass splits in the more neutron-deficient Fm isotopes and results in higher values of $\bar{T}_{KE}(M')$. The values of $\bar{T}_{KE}(M')$ and $\sigma_{TKE(M')}$ for provisional masses (crosses in Fig. 10) indicate the same general trend with mass as do the values for masses corrected for neutron emission (plotted as circles).

The occurrence of peaks in the $\sigma_{TKE(M')}$ distribu-

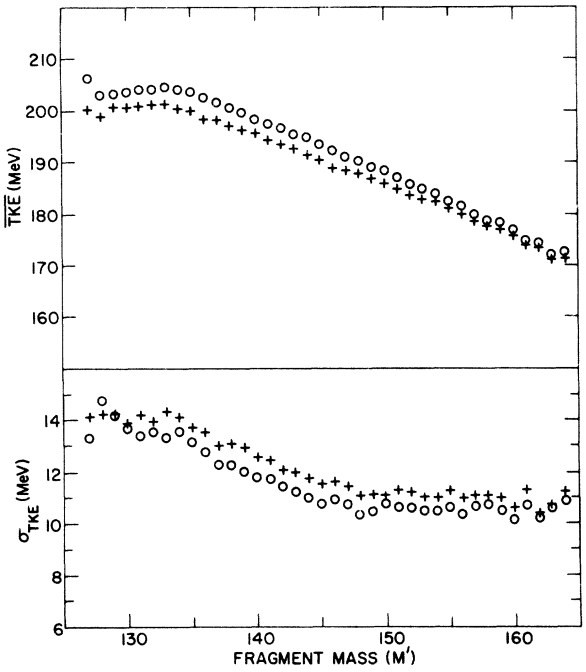

FIG. 10. The average total kinetic energy $\overline{T}_{KE}$ and the standard deviation of the total-kinetic-energy distribution σ_{TKE} as a function of mass for ^{254}Fm(sf). The distributions represented by circles are uncorrected for experimental dispersion. The crosses represent values of $\overline{T}_{KE}$ and σ_{TKE} for provisional masses.

tion as a function of mass has been qualitatively explained[23] as the result of comparable contributions to the formation of a given mass split from configurations of different total deformation. Values of $\sigma_{TKE(M')}$ (shown as circles in Fig. 10) tend to level off at masses below $M' = 134$ and then to increase from $M' = 131$ to $M' = 128$. Structure in the $\sigma_{TKE(M')}$ distribution near mass 130 has been observed in other fissioning systems and is probably the result of competing deformed-shell configurations at this mass or its complement.[23]

For ^{255}Fm(n,f) it has been shown that the provisional mass distribution determined as a function of T_{KE} is single-humped for T_{KE} values ≥ 220 MeV, indicative of symmetric fission.[5] It should be noted that since the Q values for near-symmetric fission are greater than for other fission events the probability for observing a high T_{KE} fission event near symmetry is greater than the probability for observing such an event with another mass split (see Fig. 10). Therefore, by selecting fission events with high T_{KE} one naturally selects events closely related to symmetry. A less biased selection is obtained by sorting events according to the difference in energy between the total kinetic energy of the event $T_{KE(M)}$ and the average total kinetic energy for all such events $\overline{T}_{KE(M)}$. However, to compare present results with those in Ref. 5 provisional mass distributions for ^{254}Fm(sf) were calculated as a function of T_{KE}. The results are shown in Fig. 11(a). The mass distributions are double-humped, characteristic of asymmetric fission, well-beyond the 220-MeV T_{KE} for which the single-humped distribution was observed in ^{255}Fm(n,f).[5] The distributions do exhibit the shift of both light- and heavy-mass peaks toward symmetry that is expected with this type of selection. The mass distributions obtained by

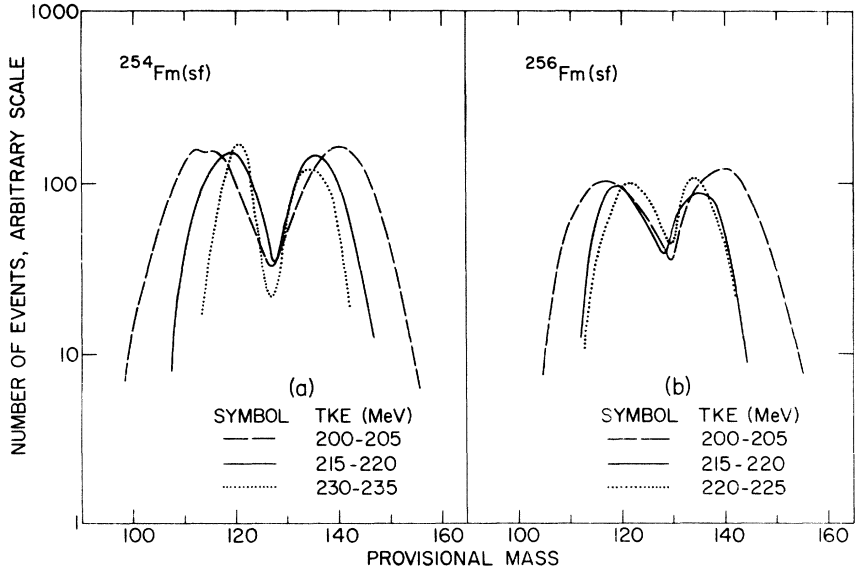

FIG. 11. Provisional mass distributions for (a) ^{254}Fm(sf) and (b) ^{256}Fm(sf) (Ref. 27) as a function of total kinetic energy.

sorting the ^{256}Fm(sf) events according to T_{KE} are shown in Fig. 11(b).[27] The double-humped mass distribution is obtained for T_{KE} events of 220–225 MeV and is discernible even for events with T_{KE} events of 220–225 MeV and is discernible even for events with T_{KE} of 225–230 MeV although the statistics are rather poor for this T_{KE} bin.[27] According to the fission model of Wilkins *et al.*[23] the mass distribution is determined near the scission point. At this point the excitation energy of the fissioning nucleus is shared between the deformation energy E_{def} and intrinsic energy E_{int} of the two fragments and is equal to the Q of the reaction plus any excitation energy, E_N, brought into the fissioning system minus the energy eventually released as kinetic energy, T_{KE}. That is,

$$E_{def} + E_{int} = Q + E_N - T_{KE} . \quad (9)$$

The total kinetic energy is dependent on the deformation of the fragments. Therefore, if one compares the ^{256}Fm(sf) and ^{255}Fm(n,f) systems for the same T_{KE} and hence for the same E_{def}, one observes from Eq. (7) that E_{int} for ^{255}Fm(n,f) is greater by E_N (~ 6 MeV)[28] than E_{int} for ^{256}Fm(sf). According to the scission-point fission model (Fig. 3 of Ref. 23) an increase in the intrinsic temperature (or energy) will change the relative stability of different shell structures. Apparently the shell structures in ^{256}Fm associated with the lowly-deformed symmetric mass split and the asymmetric mass split are very close such that the added 6 MeV in ^{255}Fm(n,f) is sufficient to change the relative stability of the two shell structures and to give rise to the single-humped mass distribution associated with $T_{KE} \geq 220$ MeV.

IV. ACKNOWLEDGMENTS

The authors wish to thank the members of Transuranium Element Production Program, Oak Ridge National Laboratory, for the einsteinium samples from which ^{254}Fm was separated, Mr. J. L. Lerner for preparation of the isotopically separated ^{254}Fm source, Dr. J. P. Unik for discussions on the handling of data, and Dr. B. D. Wilkins for help in the interpretation of the data.

---

†Work performed under the auspices of the U. S. Energy Research and Development Administration.

[1]R. Brandt, S. G. Thompson, R. C. Gatti, and L. Phillips, Phys. Rev. 131, 2617 (1963).

[2]J. P. Unik, J. E. Gindler, L. E. Glendenin, K. F. Flynn, A. Gorski, and R. K. Sjoblom, in *Proceedings of the Third IAEA Symposium on the Physics and Chemistry of Fission, Rochester, 1973* (International Atomic Energy Agency, Vienna, 1974), Vol. II, p. 19.

[3]J. P. Balagna, G. P. Ford, D. C. Hoffman, and J. D. Knight, Phys. Rev. Lett. 26, 145 (1971).

[4]W. John, E. K. Hulet, R. W. Lougheed, and J. J. Weslowski, Phys. Rev. Lett. 27, 45 (1971).

[5]R. C. Ragaini, E. K. Hulet, R. W. Lougheed, and J. Wild, Phys. Rev. C 9, 399 (1974).

[6]R. M. Harbour, K. W. MacMurdo, D. E. Troutner, and M. V. Hoehn, Phys. Rev. C 8, 1488 (1973).

[7]K. F. Flynn, E. P. Horwitz, C. A. A. Bloomquist, R. F. Barnes, R. K. Sjoblom, P. R. Fields, and L. E. Glendenin, Phys. Rev. C 5, 1725 (1972).

[8]K. F. Flynn, J. E. Gindler, R. K. Sjoblom, and L. E. Glendenin, Phys. Rev. C 11, 1676 (1975).

[9]K. F. Flynn, J. E. Gindler, and L. E. Glendenin, Phys. Rev. C 12, 1478 (1975).

[10]H. W. Schmitt, J. H. Neiler, and F. J. Walter, Phys. Rev. 141, 1146 (1966).

[11]The amount of ^{254m}Es compared with the amount of ^{253}Es, determined by α pulse analysis of the ^{253}Es and of the ^{254}Fm daughter of ^{254m}Es, was ~ 8% at approximately 40 hours after removal of the einsteinium sample from the reactor.

[12]In one catcher foil experiment (see Sec. II B) the fission activity of the ^{254}Fm decreased from >99% to 72% of the total fission activity. Appropriate corrections for ^{250}Cf(sf) to the fission produce activities observed in this measurement were based on the number of fission events attributable to ^{254}Fm and to ^{250}Cf during this experiment and on the fission yields (Ref. 13) for ^{250}Cf(sf).

[13]K. F. Flynn, J. E. Gindler, and L. E. Glendenin, J. Inorg. Nucl. Chem. 39, 759 (1977).

[14]K. F. Flynn, Argonne National Laboratory Report No. ANL 75-24, 1975 (unpublished).

[15]W. Reisdorf, J. P. Unik, H. C. Griffin, and L. E. Glendenin, Nucl. Phys. A177, 337 (1971).

[16]B. R. Erdal, J. C. Williams, and A. C. Wahl, J. Inorg. Nucl. Chem. 31, 2993 (1969).

[17]K. F. Flynn, J. E. Gindler, and L. E. Glendenin, J. Inorg. Nucl. Chem. 37, 881 (1975).

[18]F. Manero and V. A. Konshin, Atom. Energ. Rev. 10, 637 (1972).

[19]K. Wolfsberg and G. P. Ford, Abstracts of Papers, American Chemical Society, 167th National Meeting, Los Angeles, California, March 31–April 5, 1974 (unpublished) NUCL-21.

[20]K. Flynn, J. Gindler, L. Glendenin, A. Gorski, R. Sjoblom, and J. Unik, Abstracts of Papers, American Chemical Society, 167th National Meeting, Los Angeles, California, March 31–April 5, 1974 (unpublished), NUCL-22.

[21]K. F. Flynn, J. E. Gindler, L. E. Glendenin, and R. K. Sjoblom, J. Inorg. Nucl. Chem. 38, 661 (1976).

[22]M. Dakovskii, Yu. A. Lazarev, and Yu. Ts. Oganesyan, Yad. Fiz. 16, 1167 (1972) [Sov. J. Nucl. Phys. 16, 641 (1973)].

[23]B. D. Wilkins, E. P. Steinberg, and R. R. Chasman, Phys. Rev. C 14, 1832 (1976).

[24]H. R. Bowman, J. C. D. Milton, S. G. Thompson, and

W. J. Swiatecki, Phys. Rev. 129, 2133 (1963).
[25]R. Vandenbosch, Nucl. Phys. 46, 129 (1963).
[26]H. W. Schmitt, W. E. Kiker, and C. W. Williams, Phys. Rev. 137, B837 (1965).
[27]J. E. Gindler, L. E. Glendenin, and J. P. Unik, Argonne National Laboratory, unpublished data.
[28]P. A. Seeger, Nucl. Phys. 25, 1 (1961).